JOURNAL OF COMPUTATIONAL PHYSICS 63, 283–310 (1986)

An Implicit–Explicit Hybrid Method for Lagrangian Hydrodynamics

BRUCE A. FRYXELL*

Lick Observatory/Board of Studies in Astronomy and Astrophysics, University of California, Santa Cruz, California 95064

PAUL R. WOODWARD†

University of California, Lawrence Livermore National Laboratory, Livermore, California 94550

PHILLIP COLELLA

Lawrence Berkeley Laboratory, University of California, Berkeley, California 94720

AND

KARL-HEINZ WINKLER‡

Max–Planck–Institut fur Physik and Astrophysik, Institute fur Astrophysik, Garching b. Munchen, West Germany

Received May 4, 1984; revised April 2, 1985

We describe a new implicit-explicit hybrid method for solving the equations of hydrodynamics. The scheme is an extension of the explicit second-order piecewise-parabolic method (PPM) which is unconditionally stable. The scheme is thus of the Godunov type. It is conservative, accurate to second order in both space and time, and makes use of a nonlinear Riemann solver to obtain fluxes of the conserved quantities. The hybrid character of the method provides increased accuracy and computational efficiency. Switching between implicit and explicit formulations occurs smoothly and in a natural way and is performed separately for each characteristic family of waves. The method provides high resolution with shocks spread over only one zone and can produce accurate answers to most reasonable problems without the use of an artificial viscosity.

I. INTRODUCTION

In the last several years much attention has been devoted to Godunov-type methods for hydrodynamical calculations. The scheme of Godunov [1] uses non-

* Current adress: Astronomy and Astrophysics Center, University of Chicago, 5640 S. Ellis Avenue, Chicago, Illinois 60637.

† Current address: Dept. of Astronomy, University of Minnesota, Minneapolis, Minn. 55455.

‡ Current address: Los Alamos National Laboratory, Los Alamos, N.M.

0021-9991/86 $3.00

linear solutions of Riemann's shock tube problem at the interfaces between computational zones to obtain fluxes of mass, momentum, and energy between these zones during a time step. This procedure has two advantages. First, the data for the Riemann problems corresponding to the different families of waves is taken from different numerical domains of dependence chosen to match the physically correct ones as closely as possible. Second, nonlinearity can be built into the difference scheme through the Riemann solver, so that strong waves can be computed even if they are spread over only a zone or two on the grid.

The recent interest in Godunov-type methods was generated by van Leer's invention of the MUSCL scheme [2, 3]. This scheme demonstrated a means of constructing Godunov-type methods with higher than first-order accuracy. In addition, the MUSCL scheme incorporated a monotonicity constraint developed in the context of linear advection [4]. This constraint permitted the sharp shock structures characteristic of Godunov-type schemes to be computed without the introduction of the post-shock oscillations normally associated with higher-order accuracy. van Leer's MUSCL scheme has inspired the development of other more robust and more refined schemes of the Godunov type. A number of these schemes have been extensively compared to methods of a more standard type in the review of Woodward and Colella [5].

The work reported here begins with the piecewise-parabolic method (PPM) for hydrodynamics calculations. Results of PPM calcultions are compared with those of several other methods in [5] and the scheme is described in detail in [6]. In this paper we will assume that the reader is familiar with these two references. The purpose of this work is to extend the PPM scheme into the implicit regime so that it can be used to attack a much broader class of problems. In performing this extension we wish to retain the role of a Riemann solver in obtaining fluxes at the zone interfaces which are built from upstream-centered information for each characteristic family. We also desire a smooth transition at a Courant number of unity from the explicit PPM scheme to its implicit counterpart. The implicit scheme we will describe below performs this transition independently for each family of characteristics. Therefore, a wave which propagates more slowly than the mesh velocity $\Delta x/\Delta t$ will be treated by the explicit PPM scheme, while faster waves will be treated implicitly. It is our belief that one should not ask an implicit scheme to propagate steep wave fronts faster than the mesh velocity. Therefore, in the implicit portion of the scheme, we have omitted any analogs of the elaborate monotonicity constraints and contact discontinuity steepeners which allow the explicit portion of the scheme to propagate steep wave fronts so well. However, the second-order accuracy of the implicit scheme allows smooth waves to be treated without significant damping as long as they move less than about an eighth of a wavelength per time-step. We have expended considerable effort to ensure that rapidly propagating waves of short wavelength will be damped very strongly by the implicit scheme. This property gives the scheme a robustness usually associated only with much less accurate schemes employing backward Euler time differencing.

Our aim was to develop a scheme for computing transient flows containing dis-

parate timescales. Unlike many implicit schemes, which are designed to calculate steady flows, the method described in this paper was constructed primarily for problems in which time accuracy is important in at least some parts of the flow. Although the method should also work well for steady flow problems when formulated in Eulerian coordinates, it has not yet been demonstrated that using a dissipative method with second-order time accuracy is of any advantage over more conventional methods in obtaining steady state solutions.

We will present below a numerical scheme for hydrodynamical calculations which combines the following properties:

(1) smooth, automatic switching from an explicit to an implicit calculation performed separately for each characteristic family of waves,

(2) strict conservation form,

(3) construction of separate domains of dependence for each characteristic family to obtain upstream-centered information for fluxes,

(4) nonlinear solutions to Riemann's problem to compute wave interactions and allow sharp shock structures,

(5) second-order accuracy for all Courant numbers, with wave damping proportional to the Courant number in the limit of large time-steps.

Schemes for advection equations with the first property on this list have been in use for many years [7–9]. Conservative implicit schemes involving upstream centering for gas dynamics are a more recent development. Schemes of this type are now under vigorous development by the aerodynamics community (see, e.g., the collection of articles in [10, 11]). The scheme we will present below is to our knowledge the first one to possess the last property on our list, although second-order schemes employing nondissipative Crank–Nicolson time differencing are commonly used for hyperbolic problems. The combination of all five properties listed above makes the scheme presented here especially suitable as a general purpose method for solving gas dynamical problems.

II. The Linear Advection Scheme

We first describe in detail how the new scheme is applied to solve the equation for simple advection

$$\frac{\partial \rho}{\partial t} + c\frac{\partial \rho}{\partial x} = 0, \tag{1}$$

where t and x are the time and space coordinates, ρ is the quantity being advected, and c is the constant advection velocity. The space–time structure of a single zone is shown in Fig. 1, which also illustrates how the various quantities used in the following discussion are defined.

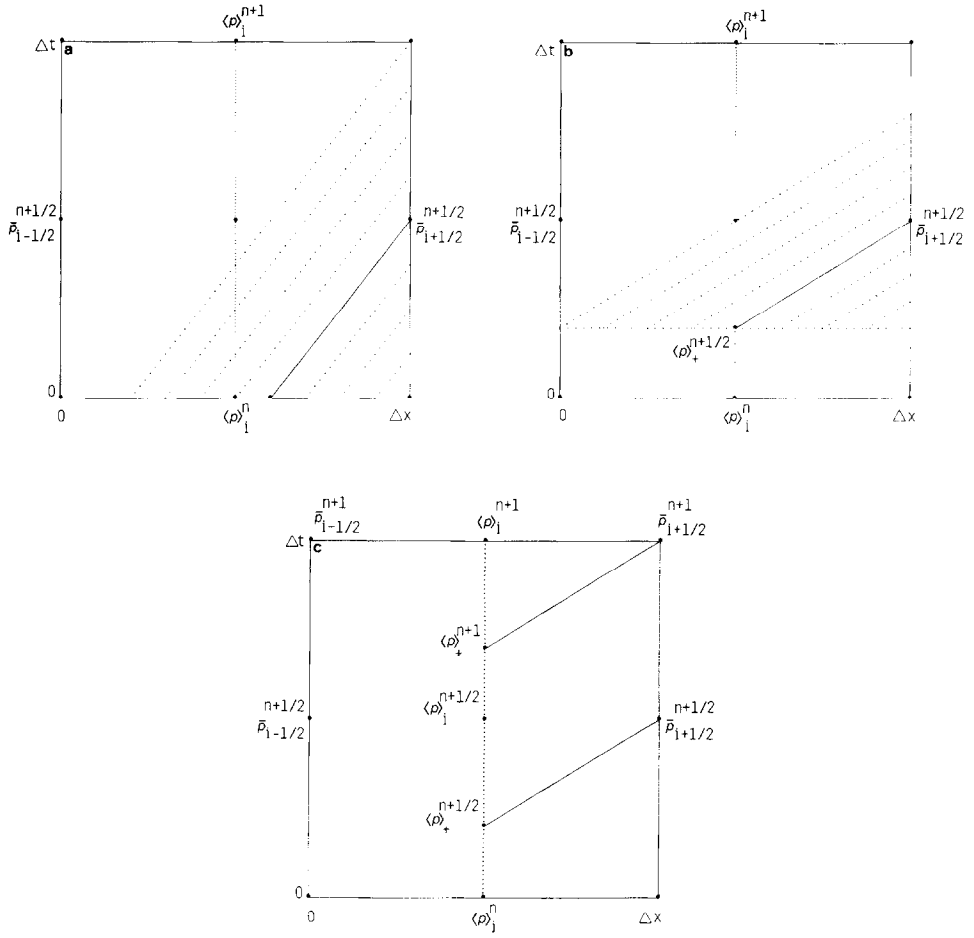

FIG. 1. The structure of zone i in space–time for three different formulations of the scheme, showing how the variables used in the text are defined. The diagonal lines represent characteristics traced backward in time to the domain of dependence of the zone interface during the time-step. The solid diagonal lines show how the spatial average of ρ over the domain of dependence is mapped onto a time-averaged value of ρ at the zone interface. For the explicit scheme (a), the domain of dependence is computed by spatial interpolation. The spatial average of ρ is then obtained by integrating the piecewise-parabolic distribution of ρ over the domain of dependence. The spatial average is mapped into an interface value time-averaged over the interval 0 to Δt. When the Courant number for the characteristic exceeds unity (b), the spatial domain of dependence extends over the entire zone and is represented by the horizontal dotted line in the figure. The value of $\langle \rho \rangle$ in this domain is obtained by interpolation in time and mapped onto the time-averaged interface value. In this case, the time-average is approximated by the average over a time interval shorter than Δt. The scheme represented by (b) is only marginally stable and is therefore not used. For the scheme which is actually used in implicit zones (c), an extra characteristic is introduced which is traced backward in time from the new time interface value. The domains of dependence are not shown in this figure, but the construction for each of the characteristics is identical to that shown in (b).

The first step is to construct a piecewise-parabolic distribution of ρ on the grid as described in [6]. The domain of dependence of the zone interface is obtained by tracing characteristics (represented by the diagonal lines in the figure). For the explicit scheme (Fig. 1a), the time-averaged value of ρ along the zone interface, $\bar{\rho}_{i+1/2}^{n+1/2}$, is then obtained by integrating the parabolic distribution of ρ over the domain of dependence of the zone edge. The value of $\langle \rho \rangle_i$ at the new time can then be obtained from

$$\langle \rho \rangle_i^{n+1} = \langle \rho \rangle_i^n - \frac{c\,\Delta t}{\Delta x} (\bar{\rho}_{i+1/2}^{n+1/2} - \bar{\rho}_{i-1/2}^{n+1/2}) \tag{2}$$

the notation $\langle \rho \rangle_i$ is used to denote the spatial average of ρ in zone i, while $\bar{\rho}$ represents a time average. This method is third-order accurate. For the case in which the Courant number

$$\sigma = \frac{c\,\Delta t}{\Delta x} \tag{3}$$

for a characteristic in a given zone is greater than 1 (Fig. 1b), the domain of dependence extends beyond the zone boundary and this method becomes unstable. In this situation a different formulation of the method must be used. The desired time average of ρ at the interface is now approximated by the average over a shorter time interval which is also centered at time $\Delta t/2$. This time average is again identified with a spatial average obtained by tracing characteristics backward in time. The spatial domain for averaging in this case is the entire zone. This average value of ρ over the zone is determined by interpolation in time. The interpolation in time to obtain $\bar{\rho}_{i+1/2}^{n+1/2}$ makes the method implicit, since the temporal distribution of $\langle \rho \rangle_i$ is not known but depends on the value of $\langle \rho \rangle_i^{n+1}$.

Linear interpolation in time between $\langle \rho \rangle_i^n$ and $\langle \rho \rangle_i^{n+1}$ for this single characteristic, as shown in Fig. 1b, yields an especially simple difference scheme. The linear interpolation function can be used in Eq. (2) to obtain an implicit expression for $\langle \rho \rangle_i^{n+1}$,

$$\langle \rho \rangle_i^{n+1} = \langle \rho \rangle_i^n - \tfrac{1}{2}[(\sigma - 1)(\langle \rho \rangle_i^{n+1} - \langle \rho \rangle_{i-1}^{n+1}) + (\sigma + 1)(\langle \rho \rangle_i^n - \langle \rho \rangle_{i-1}^n)]. \tag{4}$$

Unfortunately, this scheme is only marginally stable. Since it is important for an implicit scheme to have strong damping at large Courant numbers so that any noise generated while calculating a steady state solution can be quickly eliminated, this simple difference scheme has been rejected. Instead, we introduce a third time level at $t = \Delta t/2$ (see Fig. 1c). This doubles the number of implicit variables which must be solved for at each time step, but makes it possible to construct a scheme with more desirable properties.

The need for introducing a third time level can be understood from the following argument. Any scheme in which the flux is computed using a linear combination of the interface values at the old and new times will either be accurate only to first

order in time or not be strongly dissipative at large Courant numbers. Schemes of this type can be written in the general form

$$\rho_i^{n+1} = \rho_i^n - \sigma[(1-\beta)\,\delta\rho^{n+1} + \beta\,\delta\rho^n], \tag{5}$$

where $\delta\rho = \rho_{i+1/2} - \rho_{i-1/2}$. For $\beta = \frac{1}{2}$, the time differencing is Crank–Nicolson, while for $\beta = 0$, the method reduces to backward Euler. Frequently, a value of β slightly less than $\frac{1}{2}$ is used to provide a scheme with some damping which is "close" to second order.

In the limit of large Courant number, Eq. (5) reduces to

$$\delta\rho^{n+1} = -\frac{\beta}{1-\beta}\,\delta\rho^n. \tag{6}$$

For values of $\beta > \frac{1}{2}$, this method is unstable. For $\beta = \frac{1}{2}$ (Crank–Nicolson), $\delta\rho^{n+1} = -\delta\rho^n$ and there is no damping. When $0 < \beta < \frac{1}{2}$, there is damping in the method, but any linear wave can be damped by at most a factor $\beta/(1-\beta)$ in one time-step regardless of the size of the Courant number. Furthermore, the amount of damping in this method is independent of wavelength for large Courant numbers. To provide complete damping of a wave in a single time-step, the value of β must be 0, which results in first-order backward Euler time differencing.

Only by introducing an extra time level is it possible to obtain a scheme which is able to eliminate any unwanted noise in the solution quickly while still retaining second-order accuracy. To obtain the desired dissipation, the interface value of ρ at the old time level, $\rho_{i+1/2}^n$, is ignored in determining the flux at the interface as a function of time. The time dependence of the flux is determined by linear interpolation using only the interface values $\bar{\rho}_{i+1/2}^{n+1/2}$ and $\bar{\rho}_{i+1/2}^{n+1}$ shown in Fig. 1c. Strictly speaking, these interface values are averages over time intervals, but in constructing the time dependence of the flux we will treat them as point values at times $\Delta t/2$ and Δt. Because we will interpolate linearly in time, there will actually be no difference between these point values and the associated time averages. The approximation for $\rho_{i+1/2}$ as a function of time is therefore

$$\rho_{i+1/2}(t) = (2\bar{\rho}_{i+1/2}^{n+1/2} - \bar{\rho}_{i+1/2}^{n+1}) + \frac{2t}{\Delta t}(\bar{\rho}_{i+1/2}^{n+1} - \bar{\rho}_{i+1/2}^{n+1/2}). \tag{7}$$

As a result of using an additional time level, it is necessary to use two characteristics in each zone: one at the half time and one at the new time (see Fig. 1c). It should be emphasized that these characteristics are not traced back to the value of ρ at the zone center, but rather to the zone averaged value of ρ at the appropriate time. The domains of dependence have have not been drawn in Fig. 1c for the sake of clarity. However, the construction for each characteristic is similar to that shown in Fig. 1b for the single characteristic. The average value of ρ in the domain of dependence associated with the half-time characteristic, for example, is equal to $\langle\rho\rangle_i^n$ for $\sigma = 1$ (which matches exactly with the explicit formulation of the scheme)

and moves upward in time with increasing σ, approaching $\langle\rho\rangle_i^{n+1/2}$ for large σ. This formulation permits switching between implicit and explicit versions of the scheme at a Courant number of 1 without introducing any noise into the solution.

To derive the difference equations for the implicit scheme, we begin by integrating Eq. (1) to obtain

$$\langle\rho\rangle_i(t) = \langle\rho\rangle_i^n - \frac{c}{\Delta x}\int_0^t [\rho_{i+1/2}(\tau) - \rho_{i-1/2}(\tau)]\, d\tau, \tag{8}$$

where $\rho_{i+1/2}(\tau)$ is obtained from Eq. (7). Note that if $\rho_{i+1/2}(t)$ is obtained by linear interpolation, consistency with Eq. (8) requires that $\langle\rho\rangle_i(t)$ be interpolated quadratically in time. Combining Eqs. (3), (7), and (8) we now obtain

$$\langle\rho\rangle_i(t) = \langle\rho\rangle_i^n - \sigma\frac{t}{\Delta t}\left\{2(\bar\rho_{i+1/2}^{n+1/2} - \bar\rho_{i-1/2}^{n+1/2}) - (\bar\rho_{i+1/2}^{n+1} - \bar\rho_{i-1/2}^{n+1}) + \frac{t}{\Delta t}[(\bar\rho_{i+1/2}^{n+1} - \bar\rho_{i-1/2}^{n+1}) - (\bar\rho_{i+1/2}^{n+1/2} - \bar\rho_{i-1/2}^{n+1/2})]\right\}. \tag{9}$$

For the important special cases $t = \Delta t$ and $t = \Delta t/2$, Eq. (9) becomes

$$\langle\rho\rangle_i^{n+1} = \langle\rho\rangle_i^n - \sigma(\bar\rho_{i+1/2}^{n+1/2} - \bar\rho_{i-1/2}^{n+1/2}) \tag{10}$$

and

$$\langle\rho\rangle_i^{n+1/2} = \langle\rho\rangle_i^n - \sigma[\tfrac{3}{4}(\bar\rho_{i+1/2}^{n+1/2} - \bar\rho_{i-1/2}^{n+1/2}) - \tfrac{1}{4}(\bar\rho_{i+1/2}^{n+1} - \bar\rho_{i-1/2}^{n+1})]. \tag{11}$$

As explained above, the values of $\bar\rho_{i+1/2}^{n+1/2}$ and $\bar\rho_{i+1/2}^{n+1}$ are obtained by tracing characteristics to the zone-centered average values $\langle\rho\rangle_+^{n+1/2}$ and $\langle\rho\rangle_+^{n+1}$, respectively. Values of $\langle\rho\rangle_+^{n+1/2}$ and $\langle\rho\rangle_+^{n+1}$ are calculated by quadratic interpolation using a parabola which passes through $\langle\rho\rangle_i^n$, $\langle\rho\rangle_i^{n+1/2}$, and $\langle\rho\rangle_i^{n+1}$. It can easily be shown that the required interpolation formulae are

$$\bar\rho_{i+1/2}^{n+1} = \langle\rho\rangle_+^{n+1} = \frac{1-\sigma}{2\sigma^2}\langle\rho\rangle_i^n + \frac{2\sigma-1}{\sigma^2}\langle\rho\rangle_i^{n+1/2} + \frac{2\sigma^2-3\sigma+1}{2\sigma^2}\langle\rho\rangle_i^{n+1} \tag{12}$$

and

$$\bar\rho_{i+1/2}^{n+1/2} = \langle\rho\rangle_+^{n+1/2} = \frac{1+\sigma}{2\sigma^2}\langle\rho\rangle_i^n + \frac{\sigma^2-1}{\sigma^2}\langle\rho\rangle_i^{n+1/2} + \frac{1-\sigma}{2\sigma^2}\langle\rho\rangle_i^{n+1}. \tag{13}$$

Finally we eliminate the interface values in Eqs. (10) and (11) using Eqs. (12) and (13) to obtain

$$\langle\rho\rangle_i^{n+1} = \langle\rho\rangle_i^n - \frac{1+\sigma}{2\sigma}\Delta\langle\rho\rangle^n - \frac{\sigma^2-1}{\sigma}\Delta\langle\rho\rangle^{n+1/2} - \frac{1-\sigma}{2\sigma}\Delta\langle\rho\rangle^{n+1}, \tag{14}$$

$$\langle \rho \rangle_i^{n+1/2} = \langle \rho \rangle_i^n - \frac{2\sigma + 1}{4\sigma} \Delta \langle \rho \rangle^n - \frac{3\sigma^2 - 2\sigma - 2}{4\sigma} \Delta \langle \rho \rangle^{n+1/2} - \frac{1 - \sigma^2}{4\sigma} \Delta \langle \rho \rangle^{n+1}, \tag{15}$$

where $\Delta \langle \rho \rangle = \langle \rho \rangle_i - \langle \rho \rangle_{i-1}$. Equations (14) and (15) represent a block-bidiagonal system of linear equations which can be solved for $\langle \rho \rangle_i^{n+1}$ and $\langle \rho \rangle_i^{n+1/2}$. In zones for which $\sigma \leqslant 1$ the explicit method is used, and the matrix becomes diagonal. These zones may be omitted from the matrix inversion to reduce execution time. Note that in the limit of large Courant number, $\Delta \langle \rho \rangle^{n+1} = 3\,\Delta \langle \rho \rangle^{n+1/2} = 0$, i.e., the solution approaches the correct steady state solution $\langle \rho \rangle_i^{n+1} = \text{constant}$.

In order to derive the amplification factor for the scheme, we introduce a Fourier mode of wavenumber k so that

$$\Delta \langle \rho \rangle = (1 - s) \langle \rho \rangle, \tag{16}$$

where $s = e^{-ik\Delta x}$. After some straightforward algebra we obtain for the amplification factor

$$g = \frac{\langle \rho \rangle_i^{n+1}}{\langle \rho \rangle_i^n} = \frac{(s^2 - 1)\,\sigma + (s^2 + 6s + 1)}{2(s-1)^2\,\sigma^2 - 3(s^2 - 1)\,\sigma + (s^2 + 6s + 1)}. \tag{17}$$

It can be easily shown that the scheme is stable for $\sigma > 1$ and accurate to second order. Note in particular that for $\sigma = 1$, $\langle \rho \rangle_i^{n+1} / \langle \rho \rangle_i^n = s$, the exact solution, and at a given wavelength g approaches 0 for very large timesteps. Thus any oscillations (particularly unwanted noise) generated in the solution will be strongly damped in zones in which the Courant number is very large. Also, as desired, the shortest wavelength modes undergo the strongest damping.

The behaviour of $|g|$ as a function of Courant number is plotted in Fig. 2a for modes of several wavelengths. Each curve is labeled by the wavelength in units of Δx. All wavelengths are damped for $\sigma > 1$ and amplified for $0 < \sigma < 1$. In fact, the amplification factor becomes infinite for a wavelength of $2\Delta x$ at $\sigma = 1/\sqrt{2}$. In the large Courant number limit, all wavelengths are damped as $1/\sigma$ except for $2\Delta x$ which is damped as $1/\sigma^2$. The different behaviour of the $2\Delta x$ mode results from the first term in the numerator of Eq. (17) vanishing. Note that any mode except for $2\Delta x$ can be propagated approximately an eighth of a wavelength per time step before significant damping occurs.

For comparision, the amplification factor for a first order version of the method is plotted on the same graph (the dotted lines). This scheme is obtained by replacing $\langle \rho \rangle_{i+1/2}^{n+1/2}$ by $\langle \rho \rangle_{i+1/2}^{n+1}$ in Eqs. (10) and (11) and is equivalent to an implicit form of Godunov's method with backward time differencing. The amplification factor for a wavelength of $2\Delta x$ is 0 for the first-order method for all Courant numbers greater than 0, and therefore the curve representing this mode does not appear on the graph. The second-order scheme is able to compute a given wavelength mode at

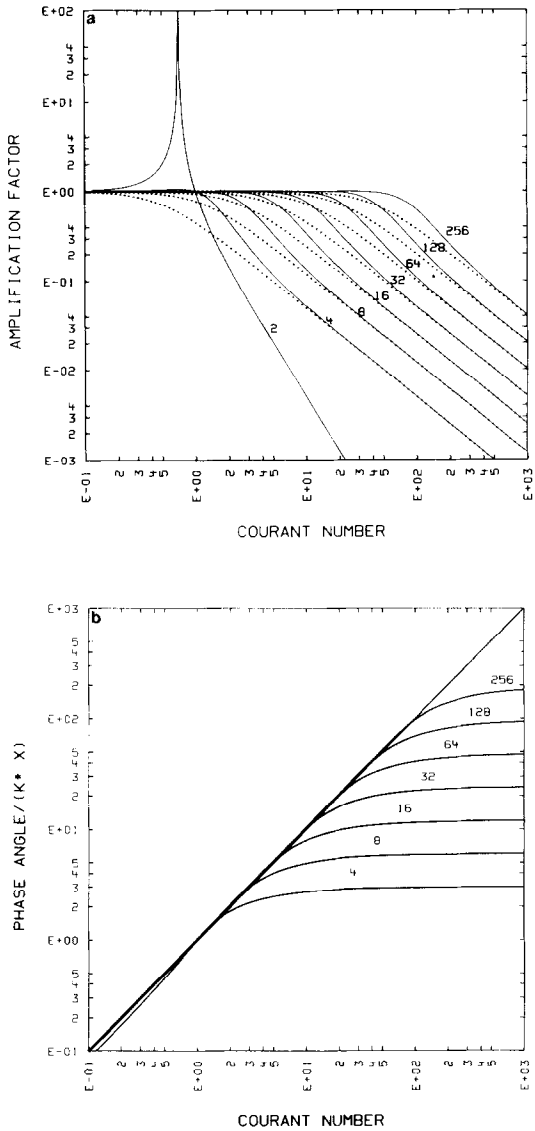

FIG. 2. (a) Amplification factor for the purely implicit second-order scheme as a function of the Courant number (the solid lines). The curves are labeled by Fourier mode wavelength in units of the zone size. For Courant numbers less than unity, the implicit scheme is unstable and the explicit formulation must be used. For comparison, the amplification factor for the first-order implicit Godunov method is also shown (dotted lines). As can be clearly seen, the second-order method is able to compute a given wavelength mode at a considerably larger Courant number before significant damping occurs. (b) Phase angle for the purely implicit second-order scheme as a function of the Courant number. Phase errors show up as departures of the curves from the diagonal line. Note that significant phase errors occur only for waves which are strongly damped.

a considerably larger Courant number without significant damping of the wave occurring. However, the dissipative properties of the two schemes are identical at large Courant numbers.

The phase angle $\phi = \tan^{-1}[-\mathrm{Im}(g)/\mathrm{Re}(g)]$ as a function of Courant number is shown in Fig. 2b. The exact solution is the diagonal line $\phi/k\Delta x = \sigma$. Significant phase errors develop only for Courant numbers for which there is strong damping.

Since the implicit scheme is stable only for $\sigma \geqslant 1$, it cannot be used for regions of the flow which require an explicit timestep. In practice, this method is combined with the explicit PPM scheme [6] to form an implicit–explicit hybrid method. The decision of which method to use is made for each characteristic in each zone. There are two advantages to using this procedure. Implicit schemes couple all the zones in the grid together, which for small timesteps is unphysical. By using the explicit method wherever possible, this error in computing domains of dependence is minimized. In addition, the implicit scheme requires much more computer time than the explicit version. As a result, by using the implicit scheme only in those zones in which the Courant number is greater than 1, the calculation can be made more efficient.

The two methods were designed specifically to join smoothly at a Courant number of 1. At first glance, it might appear that introducing an extra characteristic and an extra difference equation (Eq. (11)) suddenly when the Courant number exceeds 1 would result in a discontinuous switching between the two schemes. However, $\langle \rho \rangle_i^{n+1}$ becomes independent of $\langle \rho \rangle_i^{n+1/2}$ as σ approaches 1, as can be seen from Eq. (14). Since $\langle \rho \rangle_i^{n+1/2}$ is discarded and not used in the calculation of the next timestep, the switching is indeed continuous. Also, as discussed above, the domain of dependence used to calculate the half time interface value is the same for each scheme at $\sigma = 1$.

III. Lagrangian Hydrodynamics

The advection scheme described in the previous section can be extended for use in hydrodynamics in a way analogous to that desribed in [6] for the explicit version. The structure of a zone in space–time is as illustrated in Fig. 1, except that for Lagrangian hydrodynamics there are two characteristics at each time level (denoted in the following discussion by subscripts $+$ and $-$) corresponding to waves with characteristic speeds $+C$ and $-C$, where C is the Lagrangian sound speed. Figure 3 shows two zones in a region which contains both implicit and explicit characteristics. Average values of the hydrodynamic variables in the domain of dependence for each characteristic are interpolated and allowed to interact nonlinearly through a Riemann problem to obtain time-averaged values of the fluxes at zone interfaces.

There are two major differences between the implicit and explicit versions of the scheme. First, for implicit characteristics, as discussed for the case of advection, interpolation in time replaces the spatial iterpolation used for explicit charac-

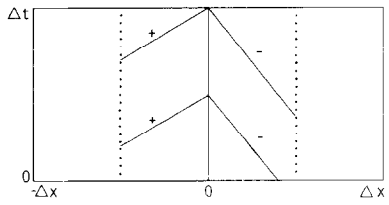

FIG. 3. The space-time structure of two adjacent zones for Lagrangian hydrodynamics. In this region of the flow, the characteristics representing waves moving to the right (marked by $a+$) are implicit while the characteristics representing waves moving to the left (marked with $a-$) are explicit. Note, however, that the minus characteristic which is traced from the new time interface value must be treated with the implicit formulation of the scheme.

teristics. The other major difference is that the implicit difference equations must be linearized. This involves computing the Jacobian of the fluxes with respect to the conserved quantities. The resulting system of linear equations is then solved by inverting a block-tridiagonal matrix.

In this paper we consider only the simple case of one-dimensional hydrodynamics in planar coordinates with a simple source term. We also limit the discussion to the case of an ideal gas equation of state, although a general equation of state can be accommodated [12, 15]. We write the equations for Lagrangian hydrodynamics in conservation form

$$\frac{\partial V}{\partial t} = \frac{\partial u}{\partial m}, \tag{18}$$

$$\frac{\partial u}{\partial t} = -\frac{\partial P}{\partial m} + G, \tag{19}$$

$$\frac{\partial E}{\partial t} = -\frac{\partial uP}{\partial} + uG, \tag{20}$$

where V is the specific volume, u is the fluid velocity, P is the pressure, E the sum of internal and kinetic energies per unit mass, G an arbitrary source term, and m the mass coordinate. The internal energy per unit mass ε, density ρ, and pressure P are related to the conserved quantities V, u, and E by

$$\varepsilon = E - \frac{u^2}{2}, \tag{21}$$

$$\rho = 1/V, \tag{22}$$

$$P = (\gamma - 1)\,\rho\varepsilon. \tag{23}$$

Equations (18)–(20) can be expressed in finite difference form as

$$U_i^{n+1} = U_i^n - \frac{\Delta t}{\Delta m}\left[F_{i+1/2}(U^n, U^{n+1}) - F_{i-1/2}(U^n, U^{n+1})\right] + \Delta t H_i(U^n, U^{n+1}), \tag{24}$$

where

$$U_i^{n+1} = \begin{pmatrix} V_1^{n+1} \\ u_i^{n+1} \\ E_i^{n+1} \\ V_i^{n+1/2} \\ u_i^{n+1/2} \\ E_i^{n+1/2} \end{pmatrix}, \qquad U_i^n = \begin{pmatrix} V_i^n \\ u_i^n \\ E_i^n \\ V_i^n \\ u_i^n \\ E_i^n \end{pmatrix}, \tag{25}$$

$F_{i+1/2}(U^n, U^{n+1})$ is the flux vector,

$$F_{i\pm 1/2}^{n+1/2} = \begin{pmatrix} -u_{i\pm 1/2}^{n+1/2} & & & \\ p_{i\pm 1/2}^{n+1/2} & & & \\ u_{i\pm 1/2}^{n+1/2} & P_{i\pm 1/2}^{n+1/2} & & \\ -\frac{3}{4}u_{i\pm 1/2}^{n+1/2} & +\frac{1}{4}u_{i\pm 1/2}^{n+1} & & \\ \frac{3}{4}p_{i\pm 1/2}^{n+1/2} & -\frac{1}{4}p_{i\pm 1/2}^{n+1} & & \\ \frac{3}{4}u_{i\pm 1/2}^{n+1/2} & P_{i\pm 1/2}^{n+1} & -\frac{1}{4}u_{i\pm 1/2}^{n+1} & P_{i\pm 1/2}^{n+1} \end{pmatrix} \tag{26}$$

and $H_i(U^n, U^{n+1})$ is the vector describing the effect of the source term

$$H_i^{n+1/2} = \begin{pmatrix} 0 \\ G_i^{n+1/2} \\ G_i^{n+1/2}\,(u_{i+1/2}^{n+1/2} + u_{i-1/2}^{n+1/2})/2 \\ 0 \\ (\frac{3}{4}G_i^{n+1/2} - \frac{1}{4}G_i^{n+1}) \\ \frac{3}{8}G_i^{n+1/2}(u_{i+1/2}^{n+1/2} + u_{i-1/2}^{n+1/2}) - \frac{1}{8}G_i^{n+1}(u_{i+1/2}^{n+1} + u_{i-1/2}^{n+1}) \end{pmatrix}. \tag{27}$$

Equation (24) represents a system of nonlinear equations which must be solved to obtain the conserved quantities at the new and half time levels. First, we proceed by linearizing the equations by expanding $F(U^n, U^{n+1})$ as

$$F(U^n, U^{n+1}) \cong F(U^n, U^n) + \left.\frac{\partial F(U^n, U^{n+1})}{\partial U^{n+1}}\right|_{U^n} \delta^{n+1}, \tag{28}$$

where $\delta^{n+1} = U^{n+1} - U^n$ and $\partial F(U^n, U^{n+1})/\partial U^{n+1}|_{U^n}$ is the Jacobian of the flux vector with respect to the new and half-time conserved quantities evaluated at the old time. A similar expansion is also performed for $H(U^n, U^{n+1})$. For convenience

we abbreviate $F_{i+1/2}(U^n, U^{n+1})$ by $F^{n+1/2}_{i+1/2}$, $F_{i+1/2}(U^n, U^n)$ by $F^n_{i+1/2}$ and similarly for H. The resulting set of linear equations can then be written as

$$\delta_i^{n+1} + \frac{\Delta t}{\Delta m}\left\{\frac{\partial F^{n+1/2}_{i+1/2}}{\partial U^{n+1}_{i+1}}\delta^{n+1}_{i+1} - \frac{\partial F^{n+1/2}_{i-1/2}}{\partial U^{n+1}_{i-1}}\delta^{n+1}_{i-1} + \left(\frac{\partial F^{n+1/2}_{i+1/2}}{\partial U^{n+1}_{1}} - \frac{\partial F^{n+1/2}_{i-1/2}}{\partial U^{n+1}_{i}}\right)\delta^{n+1}_i\right\}$$

$$-\Delta t\frac{\partial H^{n+1/2}_i}{\partial U^{n+1}_i}\delta^{n+1}_i = -\frac{\Delta t}{\Delta m}(F^n_{i+1/2} - F^n_{i-1/2}) + \Delta t\, H^n_i, \tag{29}$$

where all the derivatives are evaluated at U^n.

For problems in which iteration of the linear scheme is required to obtain improved accuracy, further iterations of Newton's method may be used. We were able to obtain satisfactory answers for all the test problems discussed in the following section without iterating. Since one extra iteration costs as much as reducing the time step by a factor of two, we suspect that for most problems, iterating is not practical.

The first step in the calculation is to obtain a piecewise-parabolic distribution of V, u, and P as described in [6]. The domain of dependence of the zone interface during the time-step for each of the two hydrodynamic wave families is then computed to obtain left and right states for the Riemann problem at the zone interface at the half-time level, as for the explicit method. For the implicit method, this procedure is performed for characteristics at both time levels. If the domain of dependence of any hydrodynamic wave extends beyond the zone boundary, the explicit method becomes unstable. In this case, the states used for the Riemann problems at both half- and new-time levels are obtained by interpolating between the zone averaged values at the old-, half-, and new-time levels (Eqs. (12) and (13)). Since the average values at the new and half time are not known, the method is implicit and requires an initial guess that the average value of each variable in the zone is constant in time. The decision of whether to use the explicit or implicit method is made for each characteristic in each zone. Thus, if one family of waves in a certain zone has a much larger velocity than the other family, the more slowly moving wave may be treated with the full accuracy of the explicit scheme. Note, however, that the characteristics traced from the new time interface value must be treated implicitly for Courant numbers greater than $\frac{1}{2}$.

We now discuss the additional steps which are necessary to perform the calculation implicitly. To calculate the Jacobian of the flux vector F, it is necessary to calculate the derivative of $u^{n+1/2}_{i+1/2}$, $P^{n+1/2}_{i+1/2}$, $u^{n+1}_{i+1/2}$, and $P^{n+1}_{i+1/2}$ with respect to the conserved quantities at both the half and new times. This is accomplished in several steps, the results of which are combined by the chain rule to produce the final answer. We begin by differentiating the equations

$$(P^* - P_\pm) \pm W_\pm(u^* - u_\pm) = \pm G_\pm\, dm_\pm, \tag{30}$$

where $W_\pm$ is the nonlinear Lagrangian wave speed

$$W_\pm = C_\pm \left(1 + \frac{\gamma+1}{2\gamma}\frac{P^* - P_\pm}{P_\pm}\right)^{1/2} \tag{31}$$

and $C_\pm$ is the Lagrangian sound speed

$$C_\pm = (\gamma P_\pm / V_\pm)^{1/2}. \tag{32}$$

The subscripts + and − refer to the states at the ends of the + and − characteristics shown in Fig. 3. The subcript * refers to the value at the zone interface at either the new or half time. Equations (30) are differentiated with respect to $u_\pm$, $P_\pm$, and $C_\pm$ to obtain

$$\frac{\partial P^*}{\partial P_\#}\left[1 \pm \frac{\partial W_\pm}{\partial P^*}(u^* - u_\pm)\right] \pm W_\pm \frac{\partial u^*}{\partial P_\#} = \left[1 \mp \frac{\partial W_\pm}{\partial P_\#}(u^* - u_\pm)\right]\delta_{\pm,\#} \pm (m^* - m_\pm)\frac{\partial G_\pm}{\partial P_\#}, \tag{33}$$

$$\frac{\partial P^*}{\partial u_\#}\left[1 \pm \frac{\partial W_\pm}{\partial P^*}(u^* - u_\pm)\right] \pm W_\pm \frac{\partial u^*}{\partial u_\#} = \pm W_\pm \delta_{\pm,\#} \pm (m^* - m_\pm)\frac{\partial G_\pm}{\partial u_\#}, \tag{34}$$

$$\frac{\partial P^*}{\partial C_\#}\left[1 \pm \frac{\partial W_\pm}{\partial P^*}(u^* - u_\pm)\right] \pm W_\pm \frac{\partial u^*}{\partial C_\#} = \mp \frac{\partial W_\pm}{\partial C_\#}(u^* - u_\pm)\delta_{\pm,\#} \pm (m^* - m_+)\frac{\partial G_\pm}{\partial C_\#}, \tag{35}$$

where # refers to either + or − and $\delta_{\pm,\#}$ is the Kronecker delta. The derivatives of the wave speeds in the above equations are

$$\frac{\partial W_\pm}{\partial P^*} = \frac{\gamma+1}{4\gamma}\frac{C_\pm^2}{P_\pm W_\pm}, \tag{36}$$

$$\frac{\partial W_\pm}{\partial P_\#} = -\frac{\gamma+1}{4\gamma}\frac{C_\#^2 P^*}{P_\#^2 W_\#}\delta_{\pm,\#}, \tag{37}$$

$$\frac{\partial W_\pm}{\partial C_\#} = \frac{W_\#}{C_\#}\delta_{\pm,\#}. \tag{38}$$

Equations (33)–(35) actually represent twelve 2×2 systems of linear equations (six at the half time and six at the new time) which can easily be solved for the desired derivatives. For any characteristic for which $\sigma < 1$, the derivatives are set equal to 0.

It is now convenient to change variables from P, u, and C to the conserved quantities V, u, and E. This can be accomplished by expressing $P_\pm$, $u_\pm$, and $C_\pm$ as functions of $V_\pm$, $u_\pm$, and $E_\pm$ using the equation of state

$$
\begin{aligned}
P_{\pm} &= \frac{\gamma-1}{V_{\pm}}\left(E_{\pm}-\frac{u_{\pm}^2}{2}\right),\\
C_{\pm} &= \frac{1}{V_{\pm}}\left[\gamma(\gamma-1)\left(E_{\pm}-\frac{u_{\pm}^2}{2}\right)\right]^{1/2},\\
u_{\pm} &= u_{\pm},
\end{aligned}
\tag{39}
$$

and differentiating to obtain

$$
\begin{aligned}
&\frac{\partial P_{\pm}}{\partial V_{\pm}} = -\frac{P_{\pm}}{V_{\pm}}, && \frac{\partial C_{\pm}}{\partial V_{\pm}} = -\frac{C_{\pm}}{V_{\pm}}, && \frac{\partial u_{\pm}}{\partial V_{\pm}} = 0,\\
&\frac{\partial P_{\pm}}{\partial E_{\pm}} = \frac{\gamma-1}{V_{\pm}}, && \frac{\partial C_{\pm}}{\partial E_{\pm}} = \frac{\gamma(\gamma-1)}{2V_{\pm}^2 C_{\pm}}, && \frac{\partial u_{\pm}}{\partial E_{\pm}} = 0,\\
&\frac{\partial P_{\pm}}{\partial u_{\pm}} = -\frac{(\gamma-1)}{V_{\pm}}u_{\pm}, && \frac{\partial C_{\pm}}{\partial u_{\pm}} = -\frac{\gamma(\gamma-1)u_{\pm}}{2V_{\pm}^2 C_{\pm}}, && \frac{\partial u_{\pm}}{\partial u_{\pm}} = 1.
\end{aligned}
\tag{40}
$$

We then obtain from Eqs. (33)–(35) and (40) using the chain rule,

$$
\begin{aligned}
\frac{\partial X^*}{\partial V_{\pm}} &= \frac{\partial X^*}{\partial P_{\pm}}\frac{\partial P_{\pm}}{\partial V_{\pm}} + \frac{\partial X^*}{\partial C_{\pm}}\frac{\partial C_{\pm}}{\partial V_{\pm}},\\
\frac{\partial X^*}{\partial u_{\pm}} &= \frac{\partial X^*}{\partial u_{\pm}} + \frac{\partial X^*}{\partial P_{\pm}}\frac{\partial P_{\pm}}{\partial u_{\pm}} + \frac{\partial X^*}{\partial C_{\pm}}\frac{\partial C_{\pm}}{\partial u_{\pm}},\\
\frac{\partial X^*}{\partial E_{\pm}} &= \frac{\partial X^*}{\partial P_{\pm}}\frac{\partial P_{\pm}}{\partial E_{\pm}} + \frac{\partial X^*}{\partial C_{\pm}}\frac{\partial C_{\pm}}{\partial E_{\pm}},
\end{aligned}
\tag{41}
$$

where X^* represents either P^* or u^*. The derivatives of X^* on the right-hand side of the equation are calculated assuming X^* is a function of $P_{\pm}$, $u_{\pm}$, and $C_{\pm}$ while the derivatives on the left-hand side of Eqs. (41) assume X^* is a function of $V_{\pm}$, $u_{\pm}$, and $E_{\pm}$.

The derivatives of the interface values with respect to $V_{\pm}$, $u_{\pm}$, and $E_{\pm}$ must now be converted to derivatives with respect to the conserved quantities at the half- and new-time levels by differentiating the interpolation formulae (Eqs. (12) and (13)) and applying the chain rule again. The derivatives of the interpolation formulae are

$$
\begin{aligned}
\frac{\partial V_{\pm}}{\partial V_i^{n+1/2}} &= \frac{2\sigma-1}{\sigma^2},\\
\frac{\partial V_{\pm}}{\partial V_i^{n+1}} &= \frac{2\sigma^2-3\sigma+1}{2\sigma^2},
\end{aligned}
\tag{42}
$$

for the new-time characteristics and

$$\frac{\partial V_{\pm}}{\partial V_i^{n+1/2}} = \frac{\sigma^2 - 1}{\sigma^2},$$
$$\frac{\partial V_{\pm}}{\partial V_i^{n+1}} = \frac{1-\sigma}{2\sigma^2}, \tag{43}$$

for the half-time characteristics with similar expressions for derivatives of $u_{\pm}$ and $E_{\pm}$. Finally, applying the chain rule gives, for example,

$$\frac{\partial u_{i\pm 1/2}^{n+1}}{\partial V_i^{n+1}} = \frac{2\sigma^2 - 3\sigma + 1}{2\sigma^2} \frac{\partial u_{i\pm 1/2}^{n+1}}{\partial V_{\pm}}, \tag{44}$$

$$\frac{\partial u_{i\pm 1/2}^{n+1}}{\partial V_i^{n+1/2}} = \frac{2\sigma - 1}{\sigma^2} \frac{\partial u_{i\pm 1/2}^{n+1}}{\partial v_{\pm}}, \tag{45}$$

$$\frac{\partial u_{i\pm 1/2}^{n+1/2}}{\partial V_i^{n+1}} = \frac{1-\sigma}{2\sigma^2} \frac{\partial u_{i\pm 1/2}^{n+1/2}}{\partial V_{\pm}}, \tag{46}$$

$$\frac{\partial u_{i\pm 1/2}^{n+1/2}}{\partial V_i^{n+1/2}} = \frac{\sigma^{2-1}}{\sigma^2} \frac{\partial u_{i\pm 1/2}^{n+1/2}}{\partial V_{\pm}}. \tag{47}$$

In the above equations, σ is computed from the zone average values at the old time. Now all that remains is to use Eqs. (44)–(47) to obtain the derivatives of the flux vector $F_{i\pm 1/2}^{n+1/2}$ and source term $H_i^{n+1/2}$. The right-hand side of Eq. (29) is calculated by evaluating Eqs. (26) and (27) at the old time (which involves solving Riemann's problem at each zone interface). The resulting matrix equation can now be inverted by standard techniques to obtain δ^{n+1} and hence U^{n+1}. The matrix is block tridiagonal with 6×6 blocks, the inversion of which completely dominates the execution time for the scheme. If desired, the procedure can now be iterated using Newton's method.

The scheme described above will provide satisfactory answers to most problems. However, when shocks are present it is advisable to make two small modifications to reduce the amplitude of the oscillations behind the shock. As a shock approaches a zone interface, it steepens into a pure jump instead of being spread over its normal width of 1 to 2 zones. Such a sharp jump will produce unwanted oscillations in the solution. To reduce this effect, the order of the scheme is reduced in zones near a shock by flattening the structure of these zones as described in [6] for the explicit scheme. The only corresponding change necessary for the implicit scheme is that the values of the fluxes and source terms in Eqs. (26) and (27) at the half-time level are replaced by a linear combination of the half-time and full-time values with coefficients determined by the flattening formula. For zones which are completely flattened, the scheme reduces to an implicit Godunov method differenced backward in time.

The other modification is the addition of a very small implicitly differenced Lapidus [13] viscosity. This is most easily accomplished by adding a term to the flux vector and modifying the Jacobian accordingly. This artificial dissipation is not used to spread the shock over several zones as in many schemes, but merely to help damp unwanted oscillations at Courant numbers near unity where the amount of dissipation in the scheme is negligible. As a result, a very small coefficient (usually about 0.1) is sufficient, so that very little diffusion of sharp structures occurs. This extra dissipation is only required when trying to push the scheme to its limit, e.g., by trying to propagate a strong shock across most of a zone in one time-step. Since a calculation of this type can be more efficiently computed with the explicit version of the scheme, the use of an artificial viscosity will not normally be required.

In order to make efficient use of this scheme, it is important to choose the value of Δt wisely. For regions of the flow which contain no discontinuities, the customary accuracy time-step control of allowing a maximum relative change in each variable may be used. Since the scheme is second order in time, a larger time-step may be used than with first-order schemes to achieve the same accuracy (see Fig. 2a). For zones containing discontinuities this choice of time-step is too restrictive. These zones can be easily detected as described in [6] and the speeds of the discontinuities estimated. The value of Δt should then be chosen so that no discontinuity moves more than one zone during the time-step.

IV. Results

The scheme was tested on a variety of problems, some of which may seem somewhat unusual for an implicit code. These calculations were chosen to illustrate the properties of the scheme as well as to show how difficult a calculation could be performed while retaining stability and an acceptable level of accuracy. The first set of calculations we discuss are of a nonlinear standing wave in a box with a reflecting wall on each side. The initial conditions were zero velocity and a sinusoidal distribution with an amplitude of 0.1 and wavelength of 25 zones for both pressure and density. The ambient pressure and density were 1.0 and 1.4, respectively. The grid contained 50 zones and the value of γ was 1.4. The calculation was performed for a variety of Courant numbers and shows how different wavelength modes are treated by the method.

Figure 4 shows the results for a Courant number of 1 (based on the ambient sound speed) plotted against the results of the purely explicit PPM code at a Courant number of 0.5. This calculation is a good test of how the implicit and explicit methods join at a Courant number of 1. As illustrated in the Courant number plot, half the wave is being treated with the implicit method and half with the explicit scheme. There is absolutely no evidence of any unwanted noise when switching from one method to the other. If any noise had been generated, it would have persisted since there is no damping in the scheme at a Courant number of 1. The results are plotted after two sound crossing times of the grid. At this time the

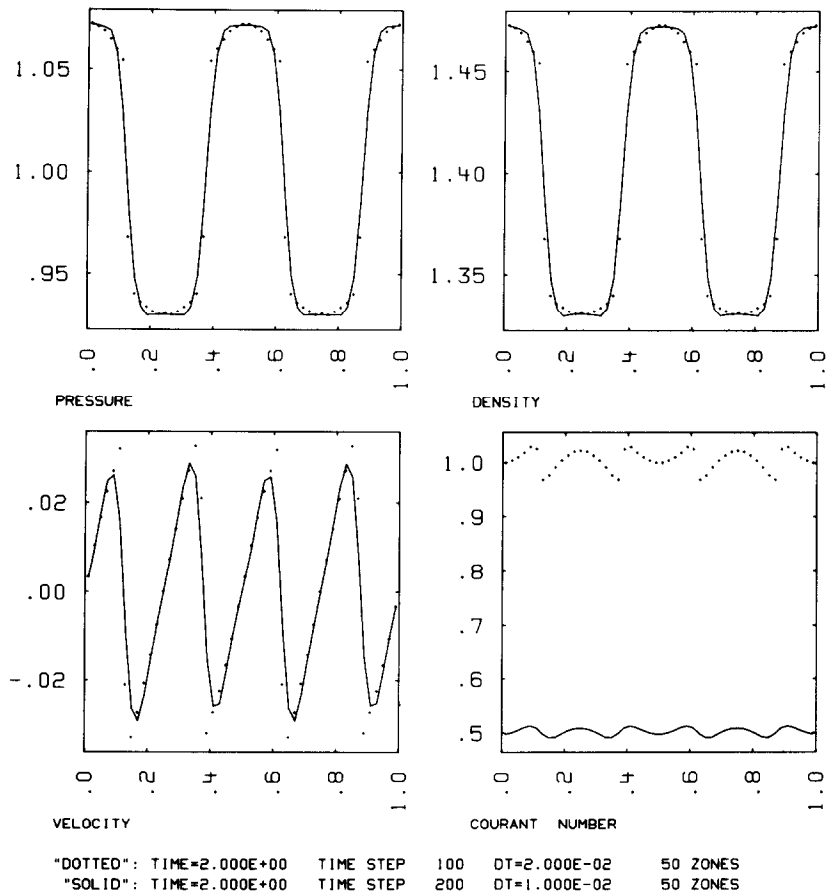

FIG. 4. Results after two sound crossing times for a nonlinear standing wave in a box with reflecting walls. The solid lines represent results obtained from the explicit version of the scheme at a Courant number of 0.5 while the dotted line was obtained using the implicit-explicit hybrid method at a Courant number of 1 based on the ambient sound speed. Note from the plot of the Courant number that half of the wave is being calculated implicitly and half explicitly without producing any noise in the solution. Since both the implicit and explicit schemes are exact at a Courant number of 1, the results obtained with the hybrid method are somewhat more accurate than those produced by the purely explicit method.

nonlinearity of the solution is clearly evident as the originally sinusoidal waves have steepened into shocks. For a linear wave, the velocity should be exactly zero at this time but for the nonlinear case, the wave traveling to the left does not exactly cancel the wave moving to the right resulting in a finite amplitude velocity wave with half the original wavelength. Note that the results at a Courant number of 1 (dotted line) are slightly more accurate than the Courant number of 0.5 results since there is somewhat less damping near a Courant number of 1. This is most apparent in the width of the shocks.

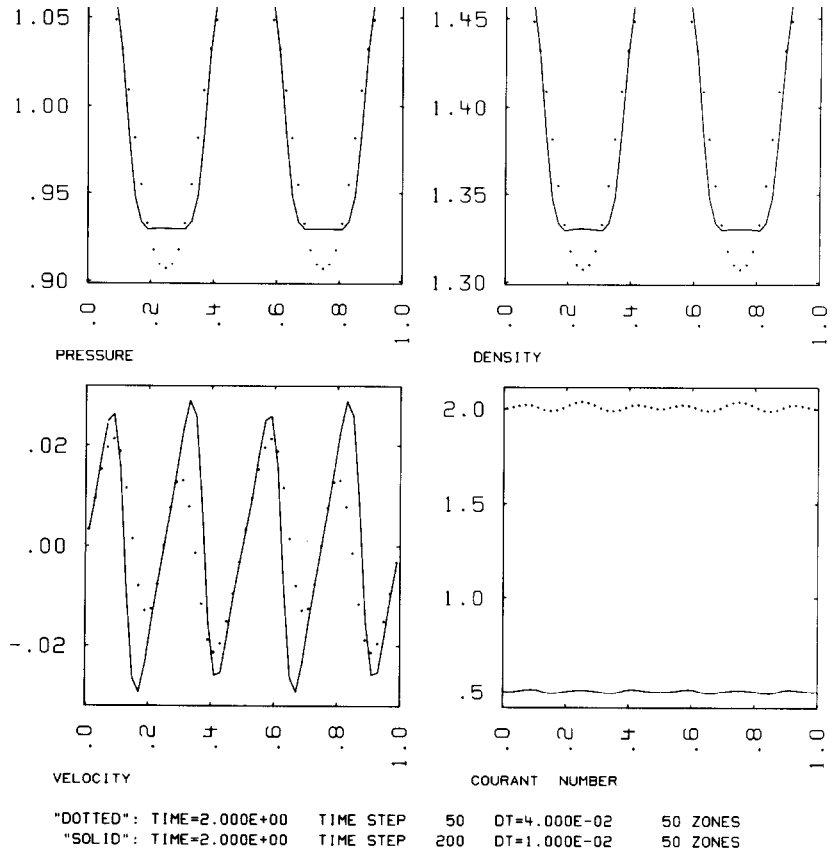

FIG. 5. Results for a nonlinear standing wave in a box obtained at a Courant number of 2. The results are still quite good with only the shortest wavelength modes being damped significantly.

The results obtained at a Courant number of 2 are shown in Fig. 5, again plotted with the results from the explicit scheme. The results are still reasonably good with only the shortest wavelength modes being damped. The nonlinearty of the solution is still clearly present, especially in the velocity. For a Courant number of 4 (Fig. 6) only the fundamental frequency remains. There is no noticeable nonlinearity left at this time and a phase error has become evident. The pressure and density should now be at their maximum amplitudes and the velocity should be 0. Figure 7 shows the results obtained at a Courant number of 25 which corresponds to the wave moving one wavelength per time step. Very strong damping has occurred, as the pressure and velocity waves have been essentially eliminated after 4 time-steps. The scheme is converging toward the steady state solution of constant pressure and zero velocity. Note that the pressure and velocity are damped before the density. A small

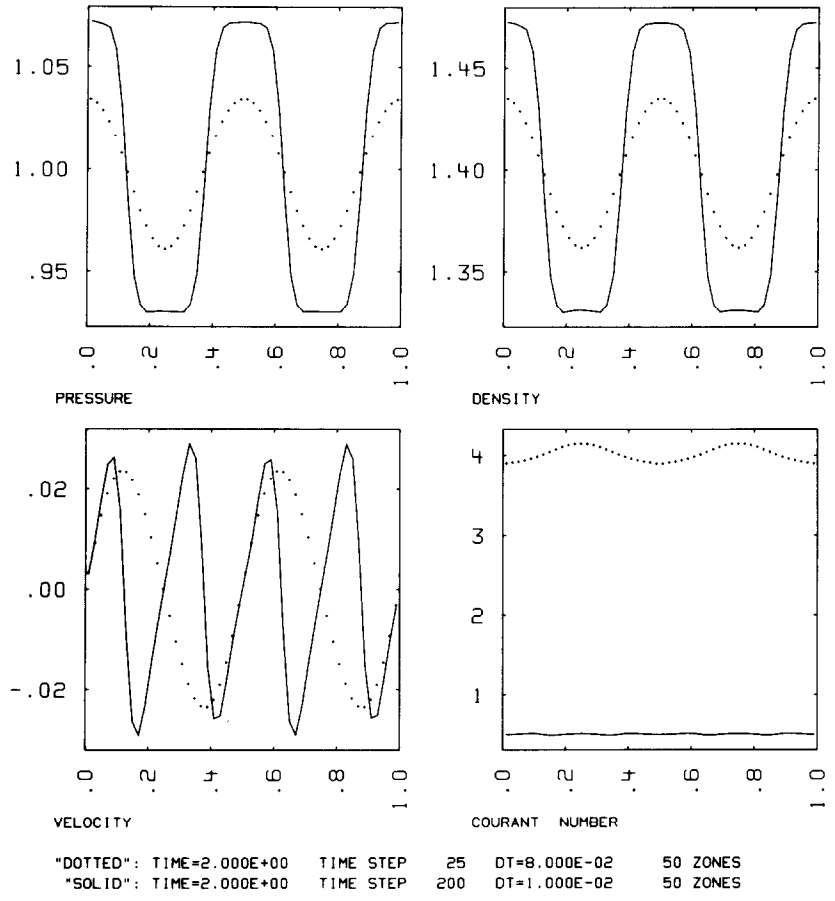

FIG. 6. Results for a nonlinear standing wave in a box obtained at a Courant number of 4. Now only the fundamental frequency remains and its amplitude has been damped noticeably.

residual oscillation of half the original wavelength remains in the density where the wave deposited its energy while being damped. This is due to the nonlinearity of the wave. Small amplitude waves can be damped in a single timestep without this effect occurring. The ability of the scheme to damp a wave this quickly is a result of discarding the value of the flux at the old time as discussed in Section II. Finally we show the results after 2 time-steps for a Courant number of 1000 in Fig. 8. The wave has been eliminated for all practical purposes but an oscillation of significant amplitude remains in the density. This is not a serious limitation of the code for practical problems, since calculating a wave with this large an amplitude at a Courant number of 1000 (the wave is moving 40 wavelengths/time-step) violates any reasonable time-step constraint one might impose. If an unwanted wave of large amplitude should appear in a calculation, it could be damped after just a few

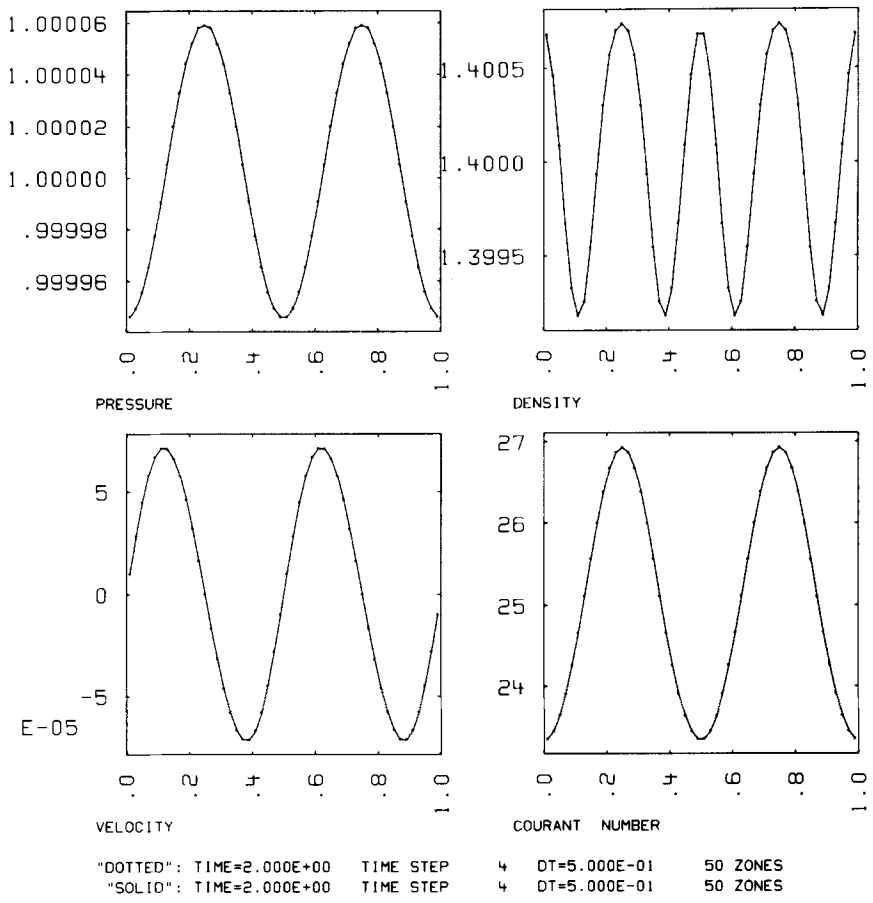

FIG. 7. Results for a nonlinear standing wave in a box obtained at a Courant number of 25. The wave is now moving 1 wavelength/time-step. As expected, the wave is strongly damped. The pressure and velocity are damped before the density, leaving an oscillation in the density of half the original wavelength where the wave deposited its energy while being dissipated.

time-steps at a smaller Courant number (e.g., $\sigma \sim 10$) and then the time-step could be increased to the desired value. Of course, to obtain the correct answer to this problem, an implicit method should not be used. We have presented these results simply to illustrate the properties of the scheme. Reasonably accurate results are obtained for $\sigma < 2$ while at large Courant numbers all wavelengths are strongly damped. This is an advantageous property for an implicit scheme, since any extraneous noise which is generated while trying to calculate a steady flow solution can be quickly eliminated.

The next class of problems we discuss is the solution of shock tubes. Again, we do not recommend the use of an implicit code for this type of problem, but include

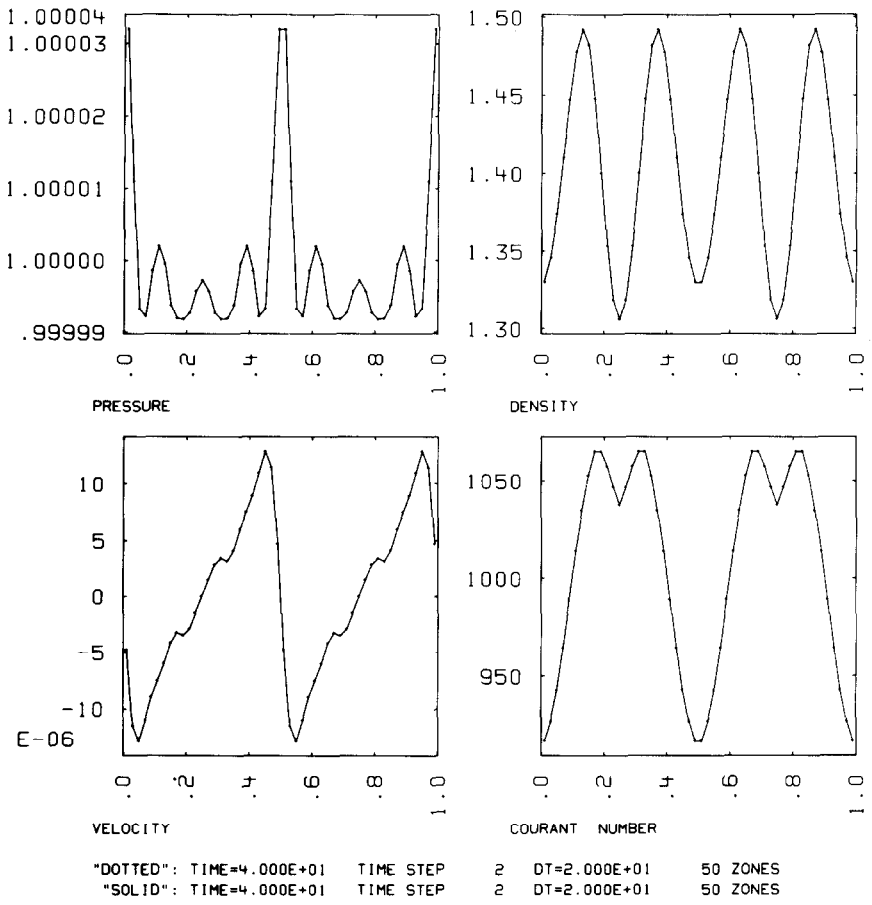

FIG. 8. Results for a nonlinear standing wave in a box obtained at a Courant number of 1000. For all practical purposes, the wave has been eliminated after two cycles except for the residual oscillation in the density. The wave is moving 40 wavelengths/time-step.

the results to show how robust and accurate the scheme is. The first shock tube calculated is the one studied by Sod [14]. The initial conditions are $\rho_L = 1$, $P_L = 1$, $u_L = 0.$, $\rho_R = 0.125$, $P_R = 0.1$, $u_R = 0.$, and $\gamma = 1.4$. The subscripts L and R refer to the states on the left and right of the initial discontinuity, which was located at zone 50 on a grid of 100 zones of equal width. The results are plotted in Fig. 9 against a very accurate solution (solid line) which was obtained with the explicit PPM code on a grid of 1000 zones. The corners of the rarefaction are quite sharp and there is only a minimal oscillation behind the shock. The maximum Courant numer (~ 1.2) occurred in the region between the shock and the contact discontinuity. The rest of the flow is calculated explicitly. The shock has moved about 0.9 zones/time-step. Even though the calculation was performed in Lagrangian coordinates, the results

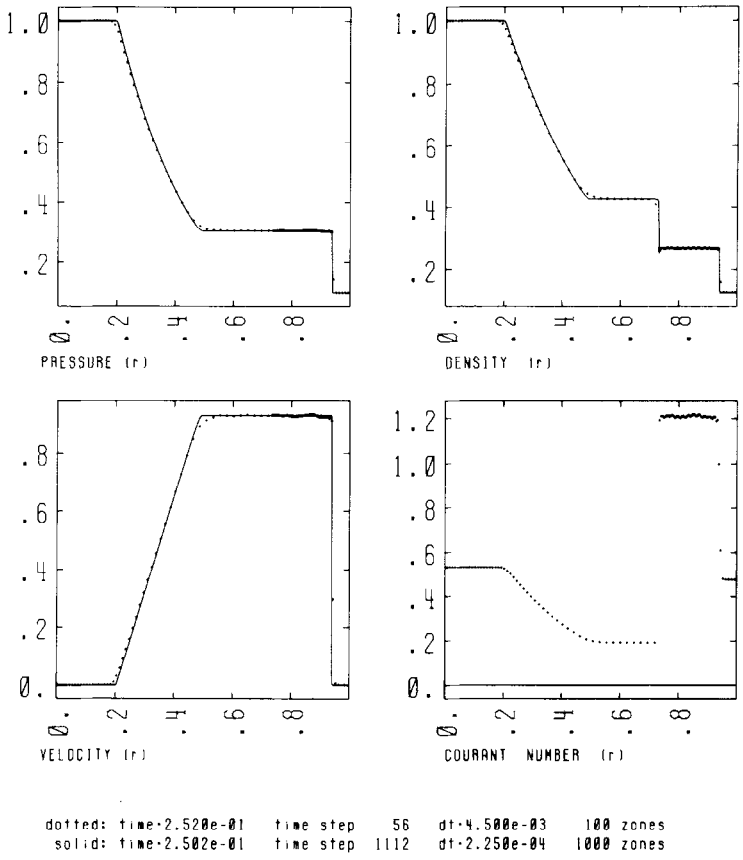

FIG. 9. Results for the shock tube studied by Sod on a grid of 100 zones. The solid line was obtained using the explicit version of the scheme with a grid of 1000 zones. There is only a slight rounding of the corners of the rarefaction and very little noise behind the shock. The region between the shock and contact discontinuity is being calculated implicitly while the rest of the flow is being computed with the explicit method. The shock is moving about 0.9 zones per timestep.

are plotted as a function of distance rather than mass to facilitate comparison with other published results (see, e.g., (16) and (17)). Even so, direct comparision is difficult. For example, the rounding at the foot of the rarefaction is exaggerated in a Lagrangian calculation since the zones in this region are expanded. Also, an Eulerian calculation will show much less noise behind the shock due to dissipation caused by the matter moving across zone boundaries. Even with these considerations, the results obtained are superior to other results we have seen of shock tube calculations performed with implicit codes, all of which were performed with smaller time-steps.

Figure 10 illustrates the results of a more difficult calculation of a shock tube containing a very strong shock with initial conditions $\rho_L = 1$, $P_L = 10^6$, $u_L = 0$,

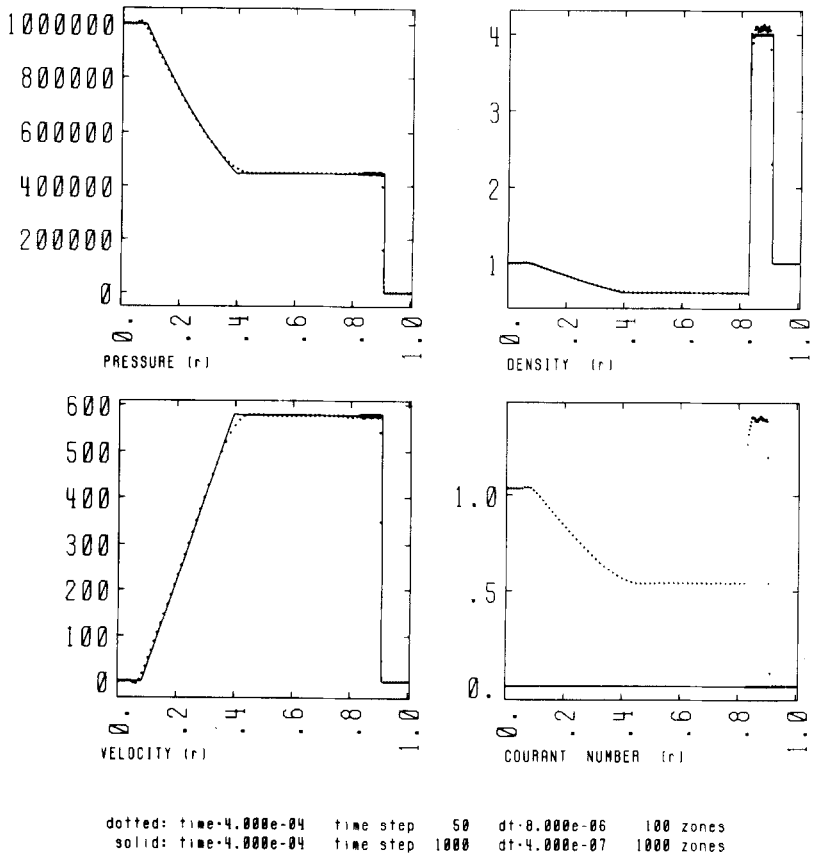

FIG. 10. Results for a shock tube problem containing a very strong shock on a grid of 100 zones plotted against an accurate solution obtained with the explicit scheme using 1000 zones. A small part of the rarefaction as well as the region between the shock and the contact are being treated implicitly. The shock is moving 0.7 zones/time-step.

$\rho_R = 1$, $P_R = 1$, $u_R = 0$, and $\gamma = \frac{5}{3}$. The initial discontinuity was placed at zone 60 on a grid of 100 zones of equal width. The results are shown at time 4×10^{-4} again plotted against the results of the explicit code on a grid of 1000 zones. The maximum Courant numer here is 1.4 and the shock is moving about 0.7 zones per time step. Note that part of the rarefaction is being calculated implicitly also with no loss of accuracy except for a small overshoot in the pressure.

We also calculated a third shock tube with parameters which are more appropriate for an implicit code. In this case there is a hot diffuse gas expanding into a cold dense gas. The sound speed in the diffuse gas is much larger than the shock speed and provides a severe time-step constraint on an explicit code. With the hybrid scheme, the shock can be calculated using the explicit portion of the code, while the region in which the sound speed is large can be treated implicitly.

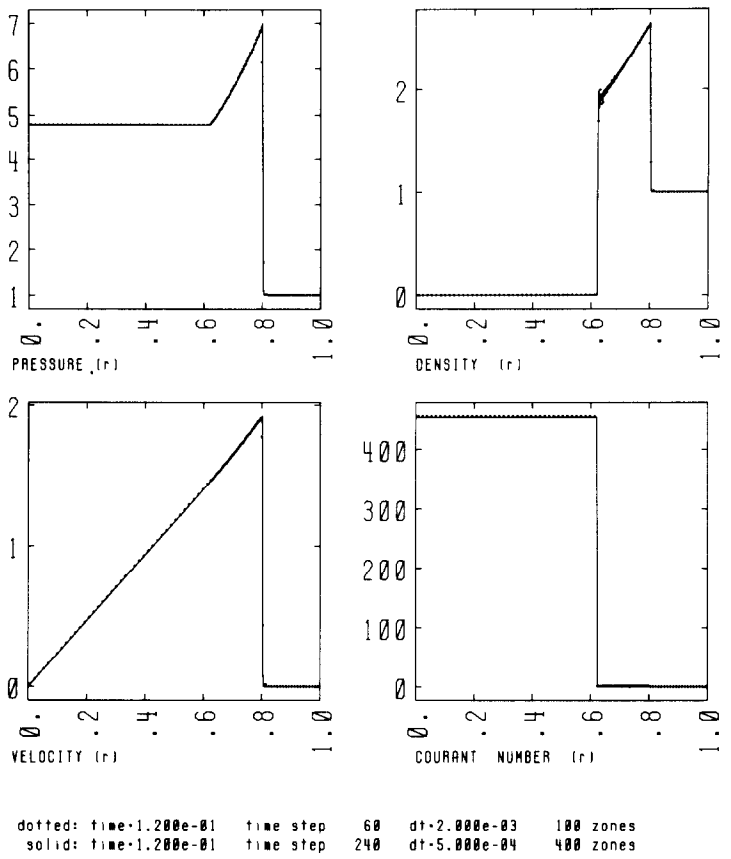

FIG. 11. Results for the expansion of a hot diffuse gas into a cold dense gas. Reflecting boundaries were used at both edges of the grid. Results obtained both with 100 zones and 400 zones are plotted. The sound speed in the diffuse gas was originally 1000 times larger than in the dense gas, resulting in a severe time-step constraint for an explicit code. With the hybrid scheme, a much larger time-step could be used. The Courant number behind the contact discontinuity originally was about 750 and has dropped to about 450 at this time. The shock is being calculated explicitly and is moving about 0.7 zones/time-step.

The initial conditions for this problem are $\rho_L = 10^{-6}$, $P_L = 10$, $u_L = 0$, $\rho_R = 1$, $P_R = 1$, $u_R = 0$, and $\gamma = \frac{5}{3}$. The initial discontinuity was located at zone 40 on a

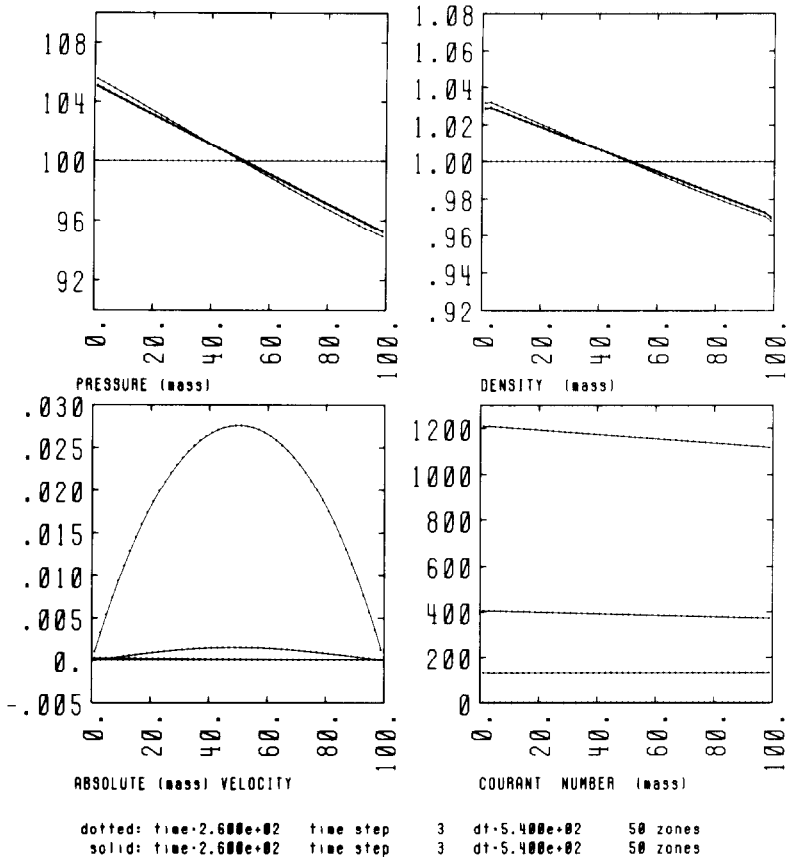

FIG. 12. The relaxation to a steady state of a uniform density gas with a constant gravitational acceleration to the left. Results after each of the first three time-steps as well as the initial distribution are plotted. The final two curves are indistinguishable, showing that the steady state has been obtained after only two time-steps.

zero velocity. The source term chosen was a constant gravitational acceleration $g = 0.1$ to the left. The grid contained 50 zones and a reflecting boundary was used on both sides. Instead of using a fixed time-step as in the previous calculations, the initial value of Δt was chosen to be 20, and the time-step was then allowed to triple after each cycle.

Figure 12 shows the initial distribution as well as the results after each of the first three cycles. The final two curves are indistinguishable showing that by the third cycle, the steady state ($\partial p/\partial m = g$) has been obtained. The calculation was continued until the Courant number exceeded 10^8 at which time the velocity had dropped to 10^{-13} and the pressure had reached the analytical solution to within the roundoff error of the computer.

V. Conclusions

We have demonstrated that the method described above provides good results in a wide variety of situations. Accurate answers can be obtained both for problems with rapidly varying solutions as well as for those with steady state solutions. The method works well for problems involving shocks of any strength and for smooth flow. The method possesses a number of advantages over other implicit methods. Most notable are: the technique of switching between implicit and explicit formulations to obtain improved accuracy and efficiency, the use of Riemann problem solutions to obtain sharp shocks and eliminate the need for artificial viscosity, and the three-level time differencing, which is superior to both the Crank–Nicolson and backward Euler methods

The algorithm can be applied equally well to any hyperbolic system of conservation laws. Although the method described above is strictly Lagrangian, an Eulerian version can be obtained by applying an explicit remap at the end of each cycle. Although there is then a time-step constraint that no material can move more than one zone/cycle, for many problems this is not restrictive. A single-step Eulerian version of the scheme which will not have this restriction as well as generalizations of the method to two dimensions, curvilinear coordinates, general equation of state, and other systems of equations will be discussed in future papers.

Acknowledgments

This work was performed in part under the auspices of the U. S. Departement of Energy by the Lawrence Livermore National Laboratory under Contract W-7404-ENG-48, the National Science Foundation Grant AST 81-08509 at the University of California at Santa Cruz, and the U. S. Department of Energy contract DE-AC03-76SF00098 at Lawrence Berkeley Laboratory. Partial support under Contract W-7405-ENG-48 was provided by the applied mathematical sciences subprogram of the Office of Energy Research.

References

1. S. K. Godunov, *Mat. Sb.* **47** (1959), 271.
2. B. van Leer, *J. Comput. Phys.* **32** (1979), 101.
3. B. van Leer and P. R. Woodward, "Proceedings TICOM Conference," Austin, Texas, 1979.
4. B. van Leer, *J. Comput. Phys.* **23** (1977), 276.
5. P. R. Woodward and P. Colella, *J. Comput. Phys.* **54** (1984), 115.
6. P. Colella and P. R. Woodward, *J. Comput. Phys.* **54** (1984), 174.
7. H. B. Keller and B. Wendroff, *Comm. Pure Appl. Math.* **10** (1957), 567.
8. S. Nakamura, "Computational Methods in Engineering and Science," pp. 175–187, Wiley, New York, 1976.
9. K. Takeuchi and A. W. Gurcak, *Trans. Amer. Nucl. Soc.* **21** (1975), 199.
10. "Proceedings of the Sixth AIAA Computational Fluid Dynamics Conference," June, 1983.
11. "Proceedings of the Euler Workshop held at INRIA," Versailles, France, December 1983.

12. P. COLELLA AND H. M. GLAZ, "Efficient Solution Algorithms for the Riemann Problem for Real Gases," Lawrence Berkeley Laboratory Report UCRL-15776, 1983.
13. A. LAPIDUS, *J. Comput. Phys.* **2** (1967), 154.
14. G. A. SOD, *J. Comput. Phys.* **27** (1978), 1.
15. P. R. WOODWARD, "Proceedings of the NATO Advanced Workshop in Astrophysical Radiation Hydrodynamics, Munich, West Germany," (K. H. Winkler and M. L. Norman, Eds.), August, 1982.
16. J. L. STEGER AND R. F. WARMING, *J. Comput. Phys.* **40** (1981), 263.
17. A. HARTEN AND H. TAL-EZER, *J. Comput. Phys.* **41** (1981), 329.